Published in final edited form as:

Nanoscale. 2017 January 26; 9(4): 1575–1579. doi:10.1039/c6nr08496f.

Dual-functional Lipid-like Nanoparticles for Delivery of mRNA and MRI Contrast Agent†

X. Luo[a], **B. Li**[a], **X. Zhang**[a], **W. Zhao**[a], **A. Bratasz**[b], **B. Deng**[c], **D. W. McComb**[c], and **Y. Dong**[a]

[a]Division of Pharmaceutics and Pharmaceutical Chemistry, College of Pharmacy, The Ohio State University, Columbus, Ohio 43210, United States

[b]Small Animal Imaging Center, The Ohio State University, Columbus, Ohio 43210, United States

[c]Center for Electron Microscopy and Analysis, Department of Materials Science and Engineering, The Ohio State University, Columbus, Ohio 43210, United States

Abstract

Multi-functional nanomaterials possess unique properties, facilitating both therapeutic and diagnostic applications among others. Herein, we developed dual-functional lipid-like nanoparticles for simultaneous delivery of mRNA and magnetic resonance imaging (MRI) contrast agent in order to express functional proteins and provide real-time visualization. TT3-Gd18 LLNs was identified as a lead formulation, which was able to encapsulate 91% of mRNA and 74% of Gd. This formulation showed comparable or slightly higher delivery efficiency of mRNA compared to the initial TT3 LLNs. Moreover, strong MRI signal was observed in cell pellets treated with TT3-Gd18 LLNs. More importantly, TT3-Gd18 LLNs demonstrated efficient delivery of mRNA and Gd contrast agent *in vivo*.

Introduction

Multi-functional nanomaterials have attracted extensive interest for a wide variety of biomedical applications, including targeted delivery, combination therapy, and theranostics.[1–7] Particularly, researchers have developed a number of theranostic platforms for both diagnosis and therapy.[8–12] Among these multi-functional carriers, lipid and lipid-like nanoparticles is one type of widely studied delivery systems.[13–19] Because of their inherent properties, they possess a number of advantages including: the capability of entrapping both hydrophilic and hydrophobic agents; efficient encapsulation of payloads; high stability and biocompatibility *in vivo*.[13, 20] To date, lipid and lipid-like nanoparticles have been applied to deliver a variety of therapeutic agents such as doxorubicin, paclitaxel, and carboplatin in combination with magnetic resonance imaging (MRI) contrast agents such as gadolinium (Gd) based contrast agents for tumor therapy and imaging.[21–24] Apart from traditional chemotherapeutic agents, plasmid DNA (pDNA) and small interfering RNA (siRNA) have also been co-loaded with MRI agents into lipid-like nanoparticles (LLNs).[25–27] For example, lipid-peptide nanocomplexes were employed to deliver both

†Electronic Supplementary Information (ESI) available. See DOI: 10.1039/x0xx00000x

Correspondence to: Y. Dong.

pDNA and Gd-chelated lipid to achieve real-time monitoring of gene therapy in the brain.[25] Multi-functional lipid-micellar nanoparticles were developed to deliver manganese (Mn) oxide and pDNA and/or doxorubicin to lungs.[26] Iron oxide nanoparticles were incorporated into lipid-like nanomaterials together with pDNA or siRNA.[27] All these multi-functional nanomaterials provide new approaches for theranostic applications.

Recently, mRNA based therapeutics has been emerging as a potential class of therapeutic agents.[28–32] Previous studies demonstrated that LLNs are promising mRNA delivery vehicles.[33–35] Herein, we designed and constructed dual-functional LLNs encapsulating both mRNA and Gd contrast agent. Gd-lipid conjugate (Gd-DTPA-BSA) was selected as the MRI agent because Gd ions are able to reduce the longitudinal relaxation time (T1) and generate bright images under magnetic fields.[36] To our knowledge, this is the first dual-functional LLNs for simultaneous delivery of mRNA and MRI contrast agent.

Results and Discussion

In order to construct dual-functional LLNs encapsulating both mRNA and MRI contrast agent, we selected TT3 LLNs, a lead nanomaterial for efficient mRNA delivery reported previously.[33] TT3 LLNs were formulated with TT3, DOPE, cholesterol (Chol) and DMG-PEG_{2000} at a molar ratio of 20/30/40/0.75. Gd-DTPA-BSA was included as an additional formulation component (Figure 1). We first formulated TT3-Gd LLNs with various molar ratios of Gd-DTPA-BSA (Table S1). Then, we characterized the properties of TT3-Gd LLNs: particle size, surface charge, and mRNA encapsulation efficiency. Particle size of TT3-Gd LLNs ranged from 103 ± 2 to 113 ± 2 nm with a PDI approximately 0.1 except TT3-Gd30 LLNs (174 ± 1 nm, PDI = 0.46) and TT3-Gd24 LLNs (159 ± 4 nm, PDI = 0.41), suggesting that a small amount of DOPE is conducive to TT3-Gd LLNs particle formulation and stability (Figure 2A). This was further confirmed by mRNA encapsulation efficiency of TT3-Gd LLNs (Figure 2C). All formulations showed slightly positive surface charge (Figure 2B). Next, we evaluated delivery efficiency of these LLNs for eGFP mRNA in Hep3B cells, a human hepatoma cell line. As shown in Figure 2D, TT3-Gd18 LLNs showed the highest eGFP signal among all the formulations. The relative eGFP expression of TT3-Gd18 LLNs is 112% of that of the initial TT3 LLNs. We then performed a correlation analysis between relative eGFP expression and particle size, zeta potential, or encapsulation efficiency, respectively (Figure S1). Relative eGFP expression was significantly correlated with mRNA encapsulation efficiency (positive correlation) and particle size (negative correlation), while no correlation was observed between eGFP expression level and particle surface charge.

The formulation TT3-Gd18 LLNs (TT3/DOPE/Gd-DTPA-BSA/Chol/DMG-PEG_{2000} = 20/12/18/40/0.75) was chosen for further *in vitro* and *in vivo* studies. Stability test showed the formulation was stable for over a month at 4 °C (Figure 3A). Cryo-transmission electron microscope (TEM) images revealed the irregular morphology of TT3-Gd18 LLNs with relatively homogenous particle size (Figure 3B). The particle size observed in the cryo-TEM was consistent with the measurements from dynamic light scattering (DLS). We then investigated the capability of TT3-Gd18 LLNs for MRI. First, we determined the Gd entrapment efficiency of TT3-Gd18 LLNs using an Inductively Coupled Plasma Sector Field Mass Spectrometer (ICP-MS). Gd entrapment efficiency was 74.14 ± 3.80% quantified from

triplicate samples (Figure S2). In order to investigate the function of the entrapped contrast agent Gd-DTPA-BSA, we performed an *in vitro* cell pellet MRI study. Cells were treated with TT3 LLNs, TT3-Gd18 LLNs at a final Gd concentration of 1.5 μM and TT3-Gd18 LLNs at a final Gd concentration of 7.5 μM, respectively. 3 h after treatment, cell pellets were imaged using a 9.4T BioSpec 94/30 superconducting magnet system as shown in Figure 3C. Consistent with the mechanism that positive contrast agents generate bright images under magnetic fields, we observed a positive correlation between cell pellet brightness and Gd concentration. Subsequently, we performed T1 mapping (T_1m) on the cell pellets. T1 relaxation time of the pellets treated with low concentration or high concentration of TT3-Gd18 LLNs was quantitatively determined to be 77.8% or 65.4% of the pellet treated with TT3 LLNs (Figure S3). These results demonstrated the capability of TT3-Gd18 LLNs for delivery of both mRNA and MRI contrast agent *in vitro*.

In order to examine the dual-function *in vivo*, TT3-Gd18 LLNs were formulated with firefly luciferase (Fluc) mRNA and injected intramuscularly (I.M) into the left leg of mice at an mRNA dose of 0.125 mg/kg, with the right leg as an untreated control (n=3). 6 h post-administration, we measured the bioluminescence intensity of both legs. A significant bioluminescence signal was detected in the TT3-Gd18 LLNs treated leg compared to the untreated leg (Figure 4A). Similarly, TT3-Gd18 LLNs was injected intramuscularly at a Gd dose of 0.6 μmol/kg (n=1). T1 weighted (T_1w) image captured 20 min after administration showed the formulation dramatically enhanced T1 signals at the injection site (Figure4B). Images captured 1 h and 6 h after administration showed moderate and weak signal enhancement, while no difference was observed in the untreated control leg (Figure 4C–D). Reflecting the above results, TT3-Gd18 LLNs are capable of delivering mRNA molecules and MRI contrast agent *in vivo*.

Conclusions

In summary, we designed and constructed dual-functional lipid-like nanoparticles for simultaneous delivery of mRNA and MRI contrast agent. This system possesses the following properties: a) providing a non-invasive imaging strategy; b) enabling image-guided mRNA delivery. Through optimizing the formulation, TT3 LLNs encapsulated 91% of mRNA and 74% of Gd. TT3-Gd18 LLNs, a lead formulation showed comparable or slightly higher delivery efficiency of mRNA compared to the initial TT3 LLNs. Meanwhile, this formulation displayed strong MRI signal in cell pellets. More importantly, consistent with *in vitro* results, TT3-Gd18 LLNs displayed efficient delivery of mRNA and Gd contrast agent in animal studies, demonstrating its dual-function. Therefore, TT3-Gd18 LLNs incorporating therapeutic mRNA and non-invasive MRI probes merit further development for theranostic applications.

Experimental Section

Materials

mRNAs encoding firefly luciferase (FLuc) and enhanced green fluorescent protein (eGFP) were purchased from TriLink Biotechnologies, Inc. (San Diego, CA). N^1,N^3,N^5-tris(3-(didodecylamino)propyl)benzene-1,3,5-tricarboxamide (TT3) was synthesized using the

method reported previously.[33] 1,2-dimyristoyl-sn-glycerol, methoxypolyethylene glycol (DMG-PEG_{2000}) was purchased from NOF America Corporation (White Plains, NY). Cholesterol was purchased from Sigma-Aldrich (St. Louis, MO). 1,2-dioleoylsn-glycero-3-phosphoethanolamine (DOPE) and (diethylenetriaminepentaacetic acid)-bis(stearylamide)-gadolinium salt (Gd-DTPA-BSA) were purchased from Avanti Polar Lipids, Inc (Alabaster, AL). Hep3B cell line was purchased from American Type Culture Collection (Manassas, VA). Eagle's Minimum Essential Medium (EMEM) was purchased from Corning Incorporated (Corning, NY). Fetal bovine serum (FBS) and Quant-iT RiboGreen RNA Assay Kit were purchased from Thermo Fisher Scientific (Waltham, MA).

Formulation of mRNA encapsulated TT3-Gd LLNs

TT3-Gd LLNs were formulated with TT3, DOPE, Gd-DTPA-BSA, Cholesterol, DMG-PEG_{2000} and mRNA (eGFP or Fluc). Briefly, TT3, DOPE, Gd-DTPA-BSA, cholesterol and DMG-PEG_{2000} were dissolved in ethanol and mixed at a molar ratio of 20:X:Y:40:0.75 based on the formulation of TT3 LLNs previously described.[33] The total molar ratio of DOPE and Gd-DTPA-BSA was maintained at 30 (X+Y=30). mRNA was diluted in 10mM citric acid buffer (pH=3). The ethanol phase was mixed with an equal volume of aqueous phase (TT3/mRNA weight ratio =10/1) and the resulting mixture was further diluted by an equivalent volume of 1× PBS buffer. The formulations were prepared via pipetting for *in vitro* studies, or using a microfluidic based mixing device (Precision NanoSystems) for *in vivo* studies.[37] All formulations prepared for *in vivo* studies were dialyzed in 1× PBS buffer using 3.5 K MWCO Slide-A-Lyzer Dialysis Cassettes (Thermo Fisher Scientific, Waltham, MA).

Characterization of mRNA encapsulated TT3-Gd LLNs

Aliquots of mRNA-LLNs were diluted in Milli-Q water. Particle size and zeta potential were determined on a NanoZS Zetasizer (Malvern, Worcestershire, U.K.). mRNA encapsulation efficiency of LLNs was measured by Quant-iT RiboGreen RNA Assay Kit following manufacturer's protocol. For stability study, the formulation was kept at 4 °C for over one month. The particle size was measured weekly using the NanoZS Zetasizer.

In vitro eGFP expression assay

Hep3B cells were cultured in EMEM supplemented with 10% heat inactivated FBS and maintained under a humidified atmosphere containing 5% CO_2 at 37 °C. Hep3B cells were seeded in 6-well plates at a density of 2.0×10^5 cells/well. After overnight incubation, cells were treated with eGFP mRNA encapsulated TT3-Gd LLNs at an mRNA amount of 150 ng. 24 h after treatment, the cells were washed, trypsinized, and collected in 1.5 ml Eppendorf tubes. Relative green fluorescence intensity was then quantified using a BD LSR II flow cytometer (San Jose, CA).

Cryo-Transmission Electron Microscopy (Cryo-TEM)

An aliquot (3 μl) of TT3-Gd18 LLNs was applied onto a 400 mesh carbon coated copper grid. The specimen grid was then blotted and immediately plunged into liquid ethane. After rapid formation of a thin film of amorphous ice, the grid was kept at liquid nitrogen

temperature and transferred to a Gatan 626 cryotransfer holder (Gatan, Pleasanton, CA). The cryo-transfer holder was loaded onto a Tecnai F20 S/TEM (FEI, Hillsboro, OR) and images were captured under low dose conditions.

Determination of Gd entrapment

Freshly formulated eGFP mRNA encapsulated TT3-Gd18 LLNs were dialyzed in 1× PBS buffer using 2.0 K MWCO Slide-A-Lyzer MINI Dialysis Devices (Thermo Fisher Scientific, Waltham, MA) to remove any unencapsulated free Gd-DTPA-BSA. 200 μl of nitric acid was added to 100 μl of dialyzed formulations to digest samples. The samples were allowed to sit in concentrated acid at RT for 1 h to fulfill complete digestion and then diluted to 10 ml total volume to make the final nitric acid concentration 2% v/v. 10 parts per billion (ppb) of Indium (In) was applied as an internal standard. Gd concentration was determined using an Inductively Coupled Plasma Sector Field Mass Spectrometer (ICP-MS, ELEMENT 2™, Thermo Fisher Scientific) and calculated through standard curves generated from Gd with predetermined concentrations.

In vitro cell pellet MRI assay

Hep3B cells were maintained in tissue culture flasks (Corning, T150) until they reached 80~90% confluency. eGFP mRNA encapsulated TT3 LLNs and TT3-Gd18 LLNs were formulated and dialyzed in 1× PBS buffer for 1 hour and 20 minutes. TT3-Gd18 LLNs were added to the flasks to reach a final Gd concentration of 7.50 μM (high conc. group) and 1.50 μM (low conc. group). TT3 LLNs served as a negative control. Cell pellets were harvested after 3 h of treatment. Both T_1w and T_1m images were acquired on a 9.4T BioSpec 94/30 superconducting magnet system (Bruker Co., Billerica, MA) with ParaVision 5.1 software. Rapid acquisition with relaxation enhancement (RARE) protocol was applied for acquiring T_1w images: repetition time (TR) / echo time (TE) = 1200 ms / 7.5 ms, rate factor = 4, 1 mm slice thickness, field of view (FOV) = 3 cm * 3 cm, matrix = 128 * 128, number of average (NA) = 1. RAREVTR (RARE with variable repetition time) protocol was applied for acquiring T_1m images: TE_Eff = 15 ms, TR = 200, 800, 1200, 1800, 3000, 5000, 10000 ms, 1 mm slice thickness, FOV = 2.3 cm * 2.3 cm, matrix = 128 * 128, NA =1. Circular ROIs with the same size were placed onto each cell pellet and T1 values were determined using ImageJ.

In vivo delivery of Fluc mRNA and Gd contrast agent

All procedures used in animal studies were approved by the Institutional Animal Care and Use Committee (IACUC) at The Ohio State University and were also consistent with local, state, and federal regulations as applicable. Fluc mRNA encapsulated TT3-Gd18 LLNs were formulated one day prior to administration and kept at 4 °C overnight after dialysis. MRI study was performed on 6–8 weeks old wild type C57BL/6 mice (The Jackson Laboratory) using the 9.4T BioSpec 94/30 system. Mice were anaesthetized with isoflurane, secured on an animal bed, and placed in a birdcage resonator which was positioned at the correct anatomical location of the animal in the MRI scanner. 50 μl of formulation (Gd dose 0.6 μmol/kg) was injected intramuscularly into the left leg of mice, leaving the right leg as an untreated control. T_1w images were captured at three different time points post-injection (20 min, 1 h, 6 h). RARE protocol used for acquiring T_1w images: TR/TE = 1500 ms / 7.5 ms,

rate factor = 4, 1 mm slice thickness, FOV = 2.8 cm * 2.8 cm, matrix = 256 * 256, NA = 2. 50 μl of formulation (mRNA dose 0.125 mg/kg) was injected similarly for bioluminescence study. 6 h after administration, mice were intraperitoneally injected with 150 μl of luciferase substrate D-luciferin (30 mg/ml) and imaged via a Xenogen IVIS imaging system (Caliper, Alameda, CA).

Supplementary Material

Refer to Web version on PubMed Central for supplementary material.

Acknowledgments

This work was supported by the Early Career Investigator Award from the Bayer Hemophilia Awards Program, Research Awards from the National PKU Alliance, New Investigator Grant from the AAPS Foundation, Maximizing Investigators' Research Award 1R35GM119679 from the National Institute of General Medical Sciences as well as the start-up fund from the College of Pharmacy at The Ohio State University.

References

1. Svenson, S., Prud'homme, RK. Multifunctional nanoparticles for drug delivery applications: imaging, targeting, and delivery. Springer Science & Business Media; 2012.
2. Bao G, Mitragotri S, Tong S. Annual review of biomedical engineering. 2013; 15:253–282.
3. Haynes MT, Huang L. Mol Ther. 2016; 24:849–851. [PubMed: 27198852]
4. Mo R, Jiang T, Di J, Tai W, Gu Z. Chemical Society Reviews. 2014; 43:3595–3629. [PubMed: 24626293]
5. Schroeder A, Heller DA, Winslow MM, Dahlman JE, Pratt GW, Langer R, Jacks T, Anderson DG. Nat Rev Cancer. 2012; 12:39–50.
6. Torchilin VP. Nature reviews Drug discovery. 2014; 13:813–827. [PubMed: 25287120]
7. Wang AZ, Langer R, Farokhzad OC. Annual Review of Medicine. 2012; 63:185–198.
8. Guthi JS, Yang SG, Huang G, Li S, Khemtong C, Kessinger CW, Peyton M, Minna JD, Brown KC, Gao J. Molecular Pharmaceutics. 2010; 7:32–40. [PubMed: 19708690]
9. Kaida S, Cabral H, Kumagai M, Kishimura A, Terada Y, Sekino M, Aoki I, Nishiyama N, Tani T, Kataoka K. Cancer Research. 2010; 70:7031–7041. [PubMed: 20685894]
10. Medarova Z, Pham W, Farrar C, Petkova V, Moore A. Nat Med. 2007; 13:372–377. [PubMed: 17322898]
11. Reddy GR, Bhojani MS, McConville P, Moody J, Moffat BA, Hall DE, Kim G, Koo YEL, Woolliscroft MJ, Sugai JV, Johnson TD, Philbert MA, Kopelman R, Rehemtulla A, Ross BD. Clinical Cancer Research. 2006; 12:6677–6686. [PubMed: 17121886]
12. Yang J, Lee CH, Ko HJ, Suh JS, Yoon HG, Lee K, Huh YM, Haam S. Angewandte Chemie International Edition. 2007; 46:8836–8839. [PubMed: 17943947]
13. Miller AD. Journal of drug delivery. 2013; 2013:165981. [PubMed: 23936655]
14. Kraft JC, Freeling JP, Wang Z, Ho RJ. Journal of pharmaceutical sciences. 2014; 103:29–52. [PubMed: 24338748]
15. Namiki Y, Fuchigami T, Tada N, Kawamura R, Matsunuma S, Kitamoto Y, Nakagawa M. Accounts of chemical research. 2011; 44:1080–1093. [PubMed: 21786832]
16. Al-Jamal WT, Kostarelos K. Accounts of chemical research. 2011; 44:1094–1104. [PubMed: 21812415]
17. Kanasty R, Dorkin JR, Vegas A, Anderson D. Nat Mater. 2013; 12:967–977. [PubMed: 24150415]
18. Pattni BS, Chupin VV, Torchilin VP. Chemical Reviews. 2015; 115:10938–10966. [PubMed: 26010257]
19. Wang Y, Miao L, Satterlee A, Huang L. Advanced Drug Delivery Reviews. 2015; 87:68–80. [PubMed: 25733311]

20. Xing H, Hwang K, Lu Y. Theranostics. 2016; 6:1336–1352. [PubMed: 27375783]
21. Na K, Lee SA, Jung SH, Shin BC. Colloids and surfaces B, Biointerfaces. 2011; 84:82–87. [PubMed: 21251801]
22. Ren L, Chen S, Li H, Zhang Z, Ye C, Liu M, Zhou X. Nanoscale. 2015; 7:12843–12850. [PubMed: 26022345]
23. Ren L, Chen S, Li H, Zhang Z, Zhong J, Liu M, Zhou X. Acta biomaterialia. 2016; 35:260–268. [PubMed: 26873364]
24. Kono K, Nakashima S, Kokuryo D, Aoki I, Shimomoto H, Aoshima S, Maruyama K, Yuba E, Kojima C, Harada A, Ishizaka Y. Biomaterials. 2011; 32:1387–1395. [PubMed: 21093041]
25. Writer MJ, Kyrtatos PG, Bienemann AS, Pugh JA, Lowe AS, Villegas-Llerena C, Kenny GD, White EA, Gill SS, McLeod CW, Lythgoe MF, Hart SL. J Control Release. 2012; 162:340–348. [PubMed: 22800579]
26. Howell M, Mallela J, Wang C, Ravi S, Dixit S, Garapati U, Mohapatra S. J Control Release. 2013; 167:210–218. [PubMed: 23395689]
27. Jiang S, Eltoukhy AA, Love KT, Langer R, Anderson DG. Nano Lett. 2013; 13:1059–1064. [PubMed: 23394319]
28. Pascolo S. Handb Exp Pharmacol. 2008; :221–235.doi: 10.1007/978-3-540-72167-3_11
29. Sahin U, Kariko K, Tureci O. Nature reviews Drug discovery. 2014; 13:759–780. [PubMed: 25233993]
30. Andries O, Kitada T, Bodner K, Sanders NN, Weiss R. Expert Rev Vaccines. 2015; 14:313–331. [PubMed: 25566800]
31. Phua KK, Nair SK, Leong KW. Nanoscale. 2014; 6:7715–7729. [PubMed: 24904987]
32. Tavernier G, Andries O, Demeester J, Sanders NN, De Smedt SC, Rejman J. J Control Release. 2011; 150:238–247. [PubMed: 20970469]
33. Li B, Luo X, Deng B, Wang J, McComb DW, Shi Y, Gaensler KM, Tan X, Dunn AL, Kerlin BA, Dong Y. Nano Lett. 2015; 15:8099–8107. [PubMed: 26529392]
34. Kauffman KJ, Dorkin JR, Yang JH, Heartlein MW, DeRosa F, Mir FF, Fenton OS, Anderson DG. Nano Lett. 2015; 15:7300–7306. [PubMed: 26469188]
35. Li B, Luo X, Deng B, Giancola JB, McComb DW, Schmittgen TD, Dong Y. Sci Rep. 2016; 6:22137. [PubMed: 26916931]
36. Liu Y, Zhang N. Biomaterials. 2012; 33:5363–5375. [PubMed: 22521487]
37. Marks JR, Placone J, Hristova K, Wimley WC. J Am Chem Soc. 2011; 133:8995–9004. [PubMed: 21545169]

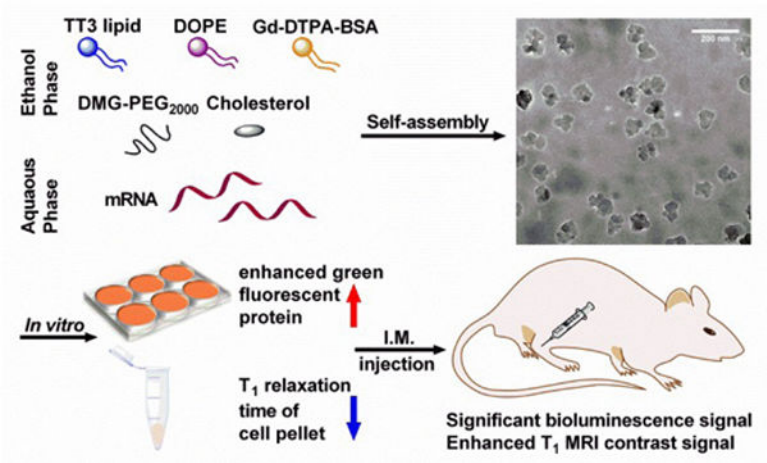

Fig. 1.

Schematic illustration of dual-functional TT3 lipid-like nanoparticles. TT3 LLNs are able to efficiently encapsulate both mRNA and Gd-DTPA-BSA through self-assembly. The resulting LLNs displayed dual-functional properties both *in vitro* and *in vivo*.

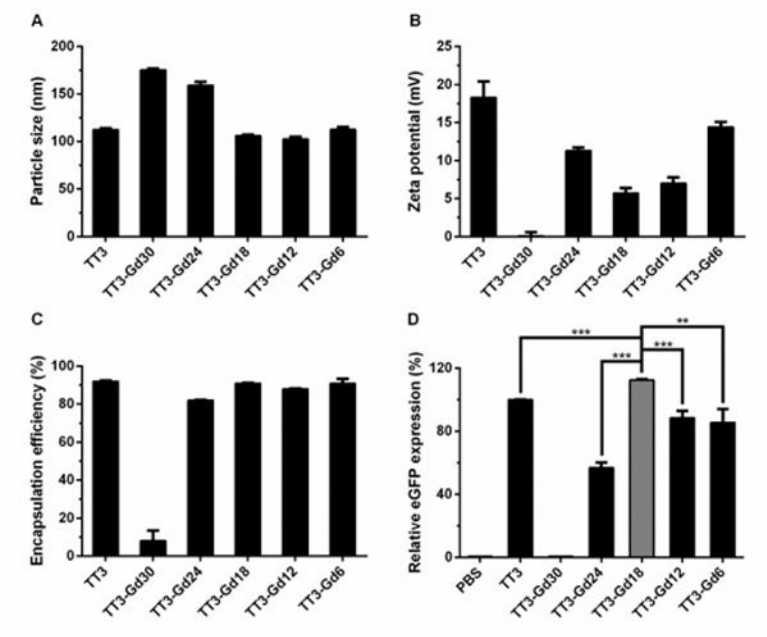

Fig. 2.

Formulation characterization and mRNA delivery of TT3-Gd LLNs. (A–C) Characterization of TT3-Gd LLNs from particle size, zeta potential, and encapsulation efficiency. (D) Delivery efficiency of eGFP mRNA. TT3-Gd18 LLNs showed significantly higher eGFP expression in Hep3B cells than other TT3 formulations. (Triplicates; two-tailed t-test; **, $P < 0.01$; ***, $P < 0.001$)higher gene silencing activity compared to other formulations. (Quadruplicates; two-tailed t-test; *, $P < 0.05$; **, $P < 0.01$; ***, $P < 0.001$)

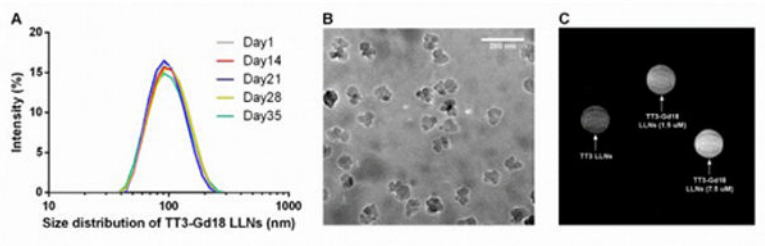

Fig. 3.

Characterization of TT3-Gd18 LLNs and *in vitro* MRI. (A) Particle size of TT3-Gd18 LLNs remained constant for over one month. (B) A representative cryo-TEM image of TT3-Gd18 LLNs. Scale bar: 200 nm. (C) A representative T1 weighted image of cell pellets.

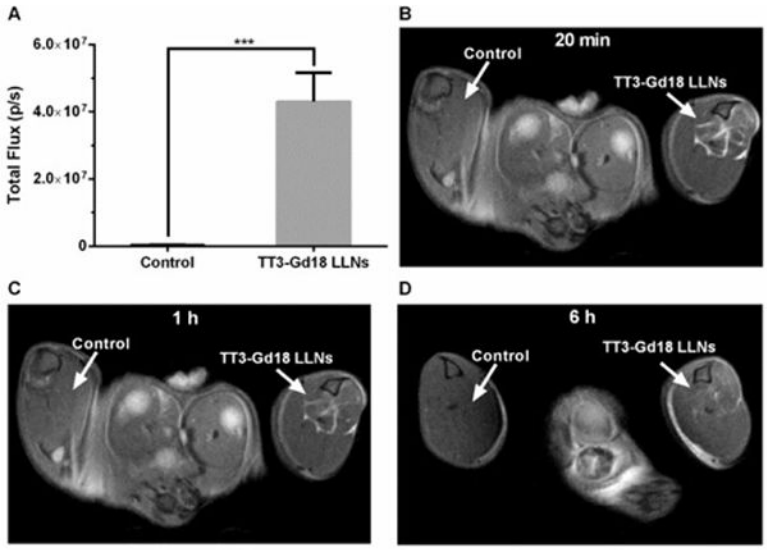

Fig. 4.

Dual-function of TT3-Gd18 LLNs *in vivo*. (A) TT3-Gd18 LLNs delivery of Fluc mRNA. A significant bioluminescence signal was observed in treated groups compared with the untreated groups (n=3). (B–D) T1 weighted images of mouse legs 20 min (B), 1 h (C), and 6 h (D) after intramuscular injection of TT3-Gd18 LLNs (n=1).